Int. J. Electrochem. Sci., 15 **(2020)** 7310 – 7325, doi: 10.20964/2020.08.50

International Journal of
ELECTROCHEMICAL
SCIENCE
www.electrochemsci.org

Stress Corrosion Behaviour of a Heating Ageing-treated Al-4.47Zn-2.13Mg-1.20Cu Alloy in the Presence of Sulfate Reducing Bacteria

Xinyi Liu[1], Chenchong Wang[2], Xu Wang[1,], Ming Wu[3,*], Liang Li[4], and Zhihao Zhao[3]*

[1] School of Mechanical Engineering, Liaoning Shihua University, Fushun, Liaoning, 113001, P. R. China
[2] State Key Laboratory of Rolling and Automation, School of Materials Science and Engineering, Northeastern University, Shenyang, Liaoning, 110819, P. R. China
[3] College of Petroleum Engineering, Liaoning Shihua University, Fushun, Liaoning, 113001, P. R. China
[4] Shenyang Aerosun-futai Expansion Joint CO., LTD, Shenyang, Liaoning, 110020, P. R. China
[*]E-mail: wangxu@lnpu.edu.cn and wuming0413@163.com

Received: 30 March 2020 / *Accepted:* 24 May 2020 / *Published:* 10 July 2020

The effect of a heating ageing treatment on the stress corrosion cracking (SCC) behaviour of an Al-4.47Zn-2.13Mg-1.20Cu (wt%) alloy in a simulated seawater solution in the presence and absence of sulfate-reducing bacteria (SRB) was studied by electrochemical techniques and stress corrosion tests. Different heating ageing treatments were applied to the samples. As the ageing rate decreased, the size of the precipitate in grain increased gradually, and the precipitate at the grain boundary displayed a progressively intermittent distribution with a narrow precipitate-free zone, which resisted stress corrosion. As the ageing rate decreased, the stress corrosion cracking susceptibility (I_{scc}) of alloy decreased, and the H10 aged samples in the sterile solution exhibited a minimum I_{scc} of 17.3%. In the SRB-inoculated solution, the impedance values of all samples were reduced, and the H10 process exhibited excellent stress corrosion cracking resistance with a low I_{scc} of 21.8%. The presence of SRB increased the SCC susceptibility due to the synergistic effect of sulfide produced by SRB metabolism, leading to hydrogen-induced cracking as the main type of stress corrosion of the alloy.

Keywords: Al-Zn-Mg-Cu alloy, heating ageing treatment, sulfate-reducing bacteria, stress corrosion

1. INTRODUCTION

Al-Zn-Mg-Cu alloys have high mechanical strength and moderate corrosion resistance, which is widely used in in the transportation industry and other fields [1-3]. Aluminium possesses a dense protective oxide film that typically forms on its surface in air to protect it from further corrosion;

however, corrosion might still occur in marine environments rich in microorganisms. A wide variety of microorganisms exist in the marine environment that attach to surfaces of devices and form biofilms, which can affect the corrosion behaviour, known as microbiologically influenced corrosion (MIC) [4]. Sulfate-reducing bacteria (SRB), which produce energy through the oxidation of organic compounds by the reduction of sulfate or other partially oxidized sulfur species to sulfide, are a major culprit contributing to MIC and have resulted in substantial losses in a wide range of industries worldwide [5]. Numerous studies have been devoted to determining the effect of SRB on the corrosion of metals, and several mechanisms have been proposed, such as cathodic depolarization by hydrogenase and sulfide, chelation of extracellular polymeric substances towards metal ions, and biocatalytic cathodic sulfate reduction [6-8]. According to Chen et al. [9], compared with the sterile medium conditions, the open-circuit potentials of the alloy shift negatively and the passivation performance worsen in the presence of the marine microbe SRB, resulting in a greater corrosion tendency, higher corrosion rate in pitting corrosion form, and a decrease in the AC impedance modulus of aluminium in the presence of the marine microbe SRB, thus reducing the polarization. Guan et al. [10] observed a significant acceleration of the corrosion rate of the 5052-aluminium alloy by SRB, and this effect was based on the consumption of hydrogen, which in return promoted SRB metabolic activity. However, this alloy is susceptible to stress corrosion cracking (SCC) due to the combined effects of stress and a corrosive solution during alloy service [11,12]. Most reports have been focused on the orrosion of Al alloy, but little is known about the effects of microorganisms on its stress corrosion behaviour. Therefore, comprehensive research on this topic is important.

An Al alloy with extraordinary corrosion resistance has been obtained using an ageing treatment [13-15]. Prasanta et al. [16] observed a reasonably high susceptibility of an Al-Zn-Mg-Cu alloys to stress corrosion cracking when aged to the T6 condition, which might seriously affect the applications. The double ageing treatment effectively improved the levels of corrosion resistance, but the peak strength was lost by 10-15% [17,18]. Baydogan et al. [19] systematically investigated the effect of retrogression and re-aging (RRA) treatment on the SCC susceptibility of 7075 aluminium alloy sheets, and after RRA treatment of 200℃ short-retrogressed, the hardness and SCC resistance of the alloy are better than that of T6 tempering state. However, the RRA process is more complex than the ordinary ageing treatment, which leads to longer production period and higher manufacturing cost [20]. A novel non-isothermal ageing treatment (NIA) has also been studied and further improved the comprehensive properties of the Al alloy [21]. The formation of the size and density of the precipitation phase must be controlled during the various steps of NIA treatments to obtain a favourable comprehensive performance. As shown in a previous study by Peng et al. [22], the maximum corrosion depth and corrosion susceptibility of an Al alloy decreases as the NIA goes on at a heating rate of 40 C/h. Jiang et al. [23] observed an increase in the corrosion resistance of an Al-Zn-Mg-Cu alloy under heating ageing conditions the corrosion resistance of by increasing the terminal temperature or reducing the heating rate. These previous studies demonstrated the potential and feasibility of using NIA to increase corrosion resistance. When both SRB and applied stress are present, their synergistic effects on the enhanced corrosion of heating ageing-treated alloys have not been reported. In the present study, the stress corrosion behaviour of the sample alloy that was processed using different heating ageing treatments and immersed in an SRB-inoculated solution was analysed. This study is important for the development of antimicrobial corrosion technology and new theoretical and practical non-isothermal ageing research.

2. EXPERIMENTAL PROCEDURES

2.1 Testing medium

The SRB strains used here were of the Desulfovibrio genus and were cultured using the standard culture medium recommended by the American Petroleum Institute [24]. The medium was composed of 0.5 g/L Na_2SO_4, 1 g/L NH_4Cl, 0.5 g/L K_2HPO_4, 0.1 g/L $CaCl_2$, 2 g/L $MgSO_4 \cdot 7H_2O$, 1 g/L yeast powder, 3.5 g/L sodium lactate, 0.1 g/L ascorbic acid, 0.1 g/L sodium hydrosulfite and 0.1 g/L $(NH_4)2Fe(SO_4)_2 \cdot 6H_2O$ [4]. All components were dissolved in deionized water at a sterile workstation. The culture medium was incubated at 121°C for 15 min for autoclaving; after cooling, the standard culture was prepared. The simulated seawater medium in this study was a 3.5 wt.% NaCl solution, which was deoxygenated by bubbling it with pure nitrogen for 0.5 h. The solution was mixed with the simulated seawater/standard culture at a ratio of 2:1 to constitute the sterile simulated seawater solution, which is referred to as the sterile solution in this article. Five millilitres of pure SRB were added to the sterile solution, and an ultraviolet spectrophotometer was used to plot the growth curve of SRB in the simulated sterile solution. The growth curve of SRB in the simulated seawater solution is shown in Figure 1. The SRB grew exponentially within five days; during this stage, the number of active SRB increased quickly. Then, the number of SRB slowly decreased and remained at a density of approximately 5×10^5 cells/mL within ten days. Thus, the pure SRB was inoculated in the sterile solution and cultured in an incubator at 30±2°C for 4 days. Then, the inoculation solution used in this paper was obtained, which is referred to as the SRB-inoculated solution. The SRB quantity was maintained at a high level during the experiment. For the sterile solution, the chilled culture and simulated seawater were mixed without inoculation with pure SRB and then were also pre-incubated for 4 days.

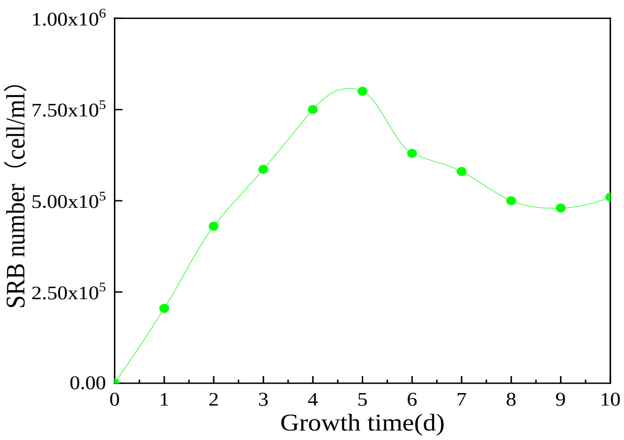

Figure 1. The amount of SRB in the simulated seawater solution.

2.2 Sample processing

A hot rolled plate of commercial aluminium alloy with a composition of 4.47% Zn, 2.13% Mg, 1.20% Cu, 0.23% Mn, 0.4% Fe, 0.072% Si, 0.036% Ti, and 0.0002% Zr (all in wt.%) was adopted. The alloy was solution-treated at 470±3°C for 1 h and then quenched with water. Next, the heating ageing treatment (HAT) process was performed. Specimens were heated from 100 to 180, 200, and 220°C at rates of 5, 10, 20, 40°C/h, for a total of 12 groups of HAT experimental conditions. Finally, the samples were cooled with water to room temperature. According to the data shown in Fig. 3, the alloy displayed the best comprehensive properties when the final ageing temperature was 200°C. For simplicity, according to the heating rate, the heating ageing treatment with the final ageing temperature of 200℃ was divided as H40, H20 and H10.

2.3 Experimental method

Microhardness tests were performed on the polished surface with a load of 200 g for 20 s using a LGTHVS-3A Vickers microhardness tester. Conductivity was measured using a Digital eddy current conductometer. At least three measurements were conducted for each specimen and then averaged to ensure the reliability of the data. The microstructures of the specimens were examined using a transmission electron microscope (TEM: JEOL-2100F) operated at 200 kV. The foils were polished to a thickness of approximately 80 μm and then electropolished in a solution of 30% nitric acid and 70% methanol at -20°C [25].

The stress corrosion cracking behaviour of the Al alloy in the sterile simulated solution and SRB-inoculated solution was determined using a LETRY WDML-30 slow strain rate tensile (SSRT) device. Prior to the experiments, the tensile specimens were sterilized by ultraviolet for 30 min and then fixed on a sealed chamber, as shown in Figure 2, and the corrosion solution was poured on it. The crevices between the chamber wall and electrode were sealed with silica gel. After soaking for 1 day in the solution, the sealed chamber was fixed on a SSRT machine. A pre-force of 400 N was applied to eliminate the crevice inside the machine and the fixture gap. Then, the strain rate was controlled at 1×10^{-6} s^{-1}, which was the recommended strain rate for SCC testing. Simultaneously, when the alloy achieved the yield strength, the electrochemical performance of the sample during fracture was tested using the PARSTAT 2273 electrochemical workstation. A saturated calomel electrode and graphite electrode were considered the reference electrode and the auxiliary electrode, respectively. A sinusoidal potential disturbance of 10 mV was applied to measure the electrochemical impedance spectroscopy (EIS) measurements in a logarithmically increasing manner in the sweep frequency range of 10^5 to 10^{-2} Hz. After sample fracture, a scanning electron microscope (SEM: TESCAN VEGA III) was used to observe morphology of the fractured alloy.

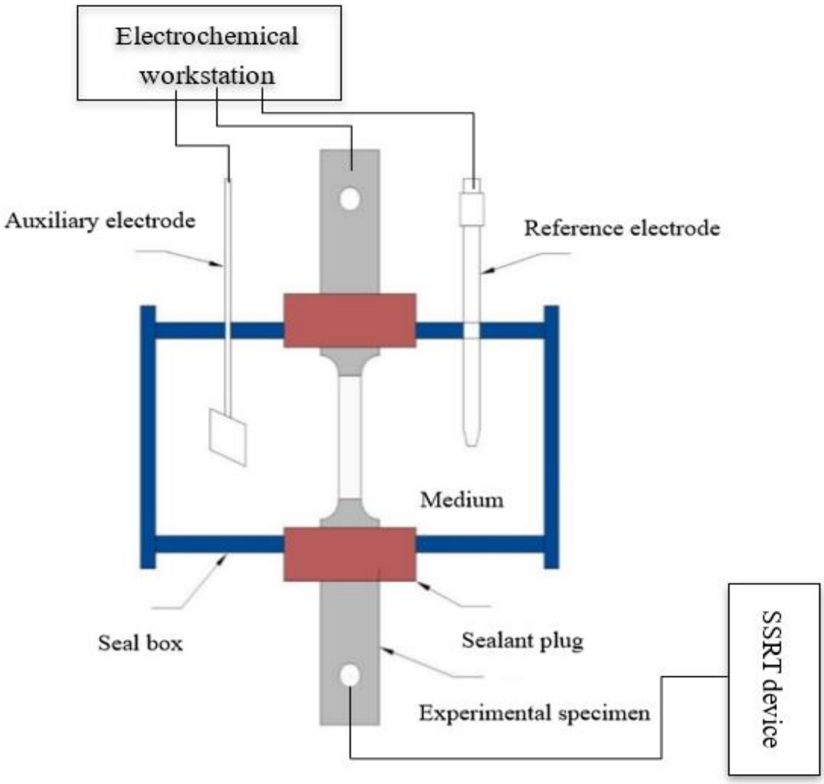

Figure 2. Schematic diagram of SSRT test equipment**.**

3. RESULTS

3.1 Hardness and conductivity

Figure 3 shows the curves of hardness and conductivity variations of the alloy during the HAT. In Fig. 3a, the hardness of alloy measured during the HAT process is greater than the alloy subjected to the T6 treatment (145 HV). At the final temperature of 180°C, the hardness of the alloy ranges from 170 to 180 HV. At a final ageing temperature of 200°C, the hardness increases rapidly with the temperature until reaching a value of 177 HV at 20°C/h, and then exhibits a slight decrease when the ageing rate increased to 40. The hardness increases with the increasing ageing rate at final temperature 220°C. In Fig. 3b, conductivity of the Al alloy decreases with the increase in the heating rate. A level of 42% IACS is obtained for HAT, which is greater than the value of 34% IACS for the T6 treatment. According to Ning et al. [26], the Al-Zn-Mg-Cu alloys with an electrical conductivity greater than or equal to 35.46% IACS display excellent resistance to stress corrosion and higher tensile strength, and samples with electrical conductivity less than or equal to 34.63% IACS present lower resistance to stress corrosion but higher tensile strength. In summary, the alloys exhibit better comprehensive mechanical properties when the final temperature is 200°C.

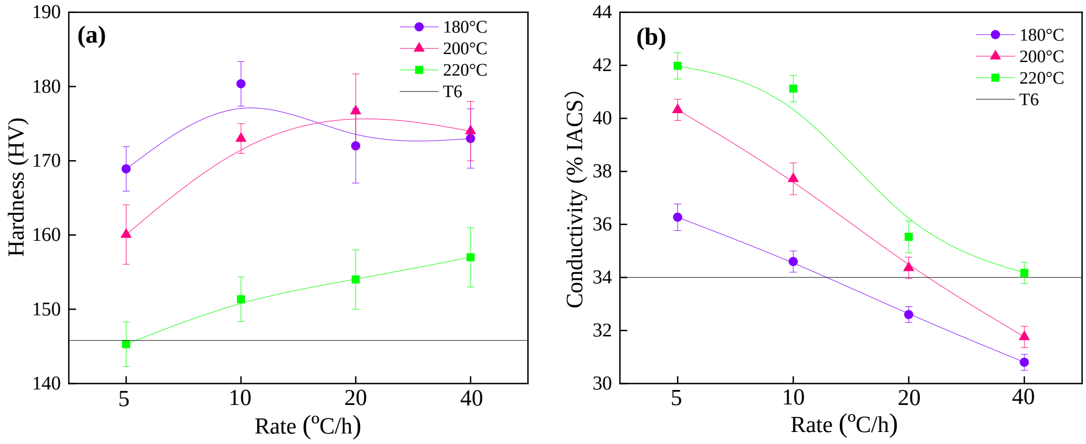

Figure 3. Hardness and conductivity variation of the Al alloy during heating aging treatment: (a) Hardness and (b) Conductivity.

3.2 Microstructures

Figure 4 presents the TEM observations of the matrix precipitates (MPs) and grain boundary precipitates (GBPs) after different ageing treatments. For the H40 treatment process, fine precipitates have been dispersed in the matrix and the grain boundary shows a discontinuous trend.

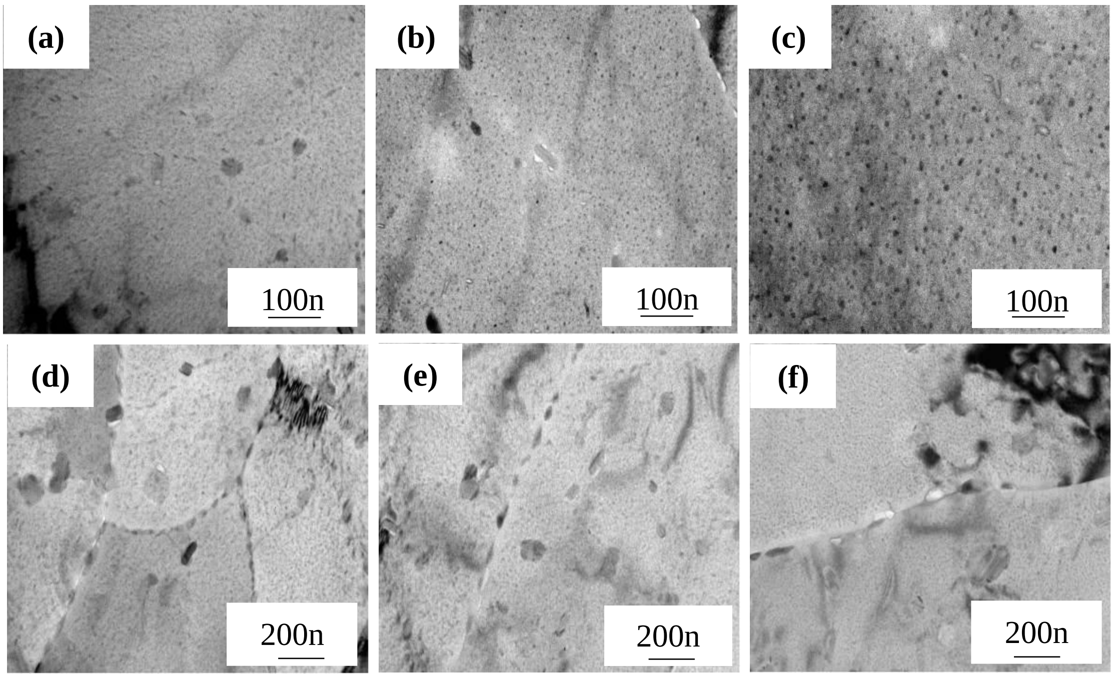

Figure 4. TEM micrographs of the alloys: (a) H40, (b) H20, (c) H10 precipitates in grain, and (d) H40, (e) H20, (f) H10 precipitates in grain boundary.

The radiuses of precipitates are significantly increased after H20, as shown in Figure 4b. Precipitates exhibit an intermittent distribution and a narrow PFZ appears to be located at the grain boundaries in the H20 sample. As the heating rate decreases, the size of MPs increases (Figure 4c) and the GBPs are distributed on the grain boundary as discrete islands with a wider PFZ (Figure 4f). Thus, as the ageing rate decreases, the size of precipitates increases, and grain boundary precipitation is gradually separated with a widened PFZ.

3.3 Electrochemical analysis

Figure 5 shows the Bode diagram of heating ageing-treated alloys in different corrosion solutions. In Fig. 5a, charge transfer resistance and solution resistance control the value of impedances at low and high frequencies, respectively [27]. At a low frequency, in sterile solution, with a decreasing ageing rate, |Z| increases and the corrosion resistance improve. In the SRB solution, the alloy subjected to the H10 treatment displays the highest impedance value, while the alloy subjected to the H40 ageing treatment has the lowest impedance value. For the same ageing-treated sample, the corrosion resistance of the sample is destroyed by sulfate-reducing bacteria. At high frequencies, the impedance value of the SRB inoculation solution is slightly lower than the sterile solution, indicating that the presence of SRB reduces the resistance of the solution. In Fig. 5b showing the Bode phase diagram, the value of phase angle is closer to 90° as the frequency in the low frequency range increases. The smallest phase angle is observed for the sample treated with H40 in the SRB solution.

The equivalent circuit diagram shown in Figure 5c is used to fit the EIS result, and the fitting data are recorded in Table 1. R_s is the solution resistance, C_f and C_t are the corrosion product capacitance and interface capacitance, respectively, and R_f and R_{ct} are the corrosion product resistance and charge transfer resistance, respectively. The resistance of the sterile solution is $46\pm1\Omega\text{•}cm^2$ and the resistance of the SRB-inoculated solution is $35\pm2\Omega\text{•}cm^2$, indicating that the electrical conductivity of SRB solution is high. In the sterile solution, with the decrease in the heating rate, the R_{ct} of the alloys are $3008\Omega\text{•}cm^2$, $5649\Omega\text{•}cm^2$, and $6211\Omega\text{•}cm^2$, respectively. The charge transfer resistance of H40, H20 and H10 samples are $2498\Omega\text{•}cm^2$, $3320\Omega\text{•}cm^2$ and $5477\Omega\text{•}cm^2$, respectively, when the SRB are present in the solution. Compared with the fitting data for the sterile solution, higher resistance characterization results in greater resistance to the electrode surface structure change, and thus the H10 ageing-treated sample in sterile solution exhibits better corrosion resistance.

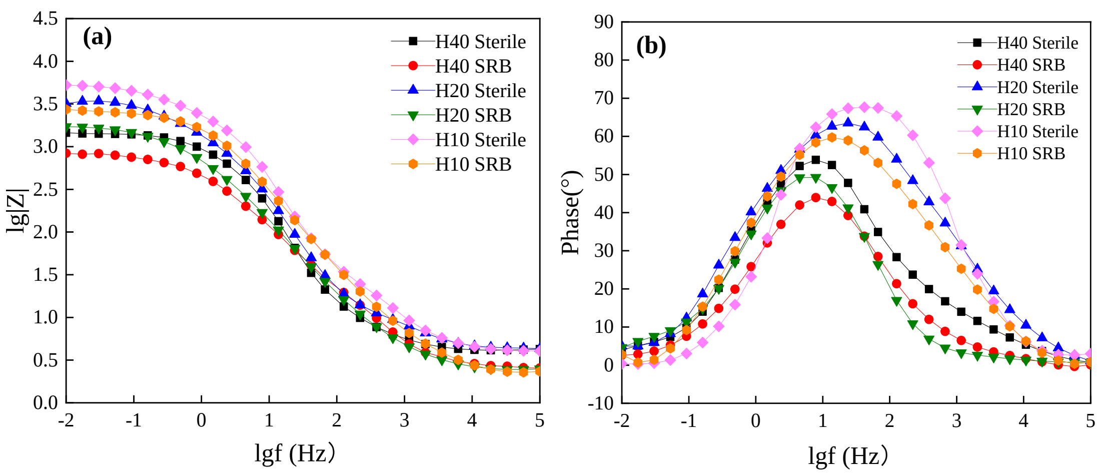

(c)

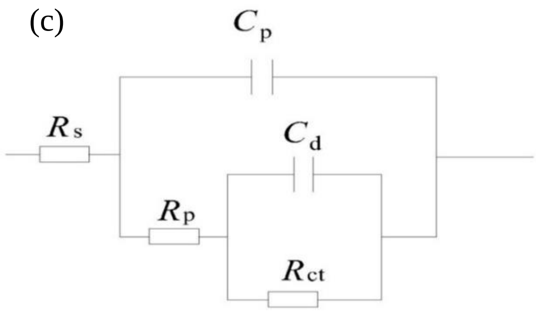

Figure 5. Bode plots of alloys after heating aging treatment in different solution: (a) |Z| diagram, (b) phase diagram, and (c) the equivalent circuit for fitting EIS.

Table 1. EIS fitting parameter of alloys after heating aging treatment in different solution.

Solution	Treatment	$R_s/\Omega\cdot cm^2$	$C_f/F\cdot cm^2$	$R_f/\Omega\cdot cm^2$	$C_t/F\cdot cm^2$	$R_{ct}/\Omega\cdot cm^2$
Sterile	H40	46.67	6.18×10^{-5}	993	2.07×10^{-5}	3008
SRB	H40	35.36	5.13×10^{-5}	1004	1.85×10^{-5}	2498
Sterile	H20	46.20	2.86×10^{-6}	1228	7.47×10^{-6}	5649
SRB	H20	36.31	5.21×10^{-6}	1168	1.09×10^{-6}	3320
Sterile	H10	46.24	8.42×10^{-6}	1536	1.85×10^{-5}	6211
SRB	H10	35.44	8.56×10^{-6}	1387	1.27×10^{-5}	5477

3.4 SSRT results

The stress-strain curves of Al-Zn-Mg-Cu alloys in different media are shown in Figure 6a. The stress-strain curves in air are used as a reference to evaluate the stress corrosion sensitivity of samples in the corrosion solution. The stress-strain curve of H40-treated samples shows that the yield strength in air, the sterile solution and SRB solution is greater than 415±10 MPa, and the elongation after fracture is 11.4%, 10.7% and 10.3%, respectively. The yield strength and elongation of samples treated with H2O heating ageing in different media are 521 MPa and 12.8% in air, 505 MPa and 12.2% in the sterile solution, and 486 MPa and 12% in the SRB-inoculated solution. The yield strength and elongation of H10-treated samples are 495 MPa and 12.5% in air, 476 MPa and 12.2% in the sterile solution, and 464 MPa and 11.8% in the SRB solution. According to the data presented above, for the ageing samples subjected to the same treatment, the yield strength of alloys in the sterile condition is obviously greater than alloys in the SRB-inoculated solution, and order of the yield strength and elongation are as follows: air > sterile solution > SRB solution. In the same medium, the alloy with the H20 treatment displays the greatest yield strength and elongation. The reduction of area (ψ) is displayed in Figure 6b. With the decrease in the ageing rate, the reduction of area of alloy in corrosion solution increases. This result confirmed that the H10 aged sample is the most corrosion-resistant alloy among the corrosion conditions.

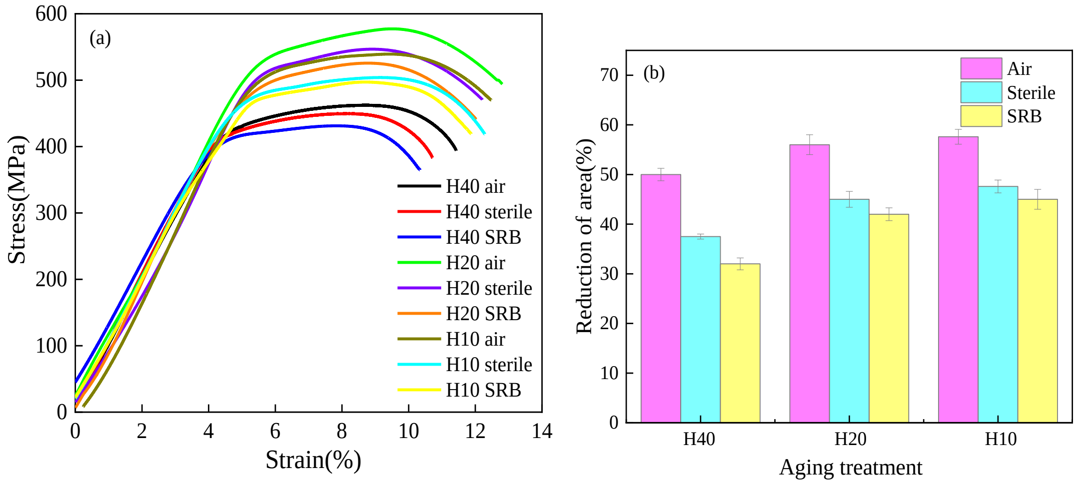

Figure 6. Stress-strain curves of heating aged alloys in different media: (a) stress-strain curves, and (b) the reduction of area.

The fracture morphology of Al-Zn-Mg-Cu alloy after SSRT in different solutions are shown in Figures 7 and 8; Fig. 7 shows the fracture morphology and Fig. 8 shows the lateral fracture morphology. The main fracture of the H40 heating ageing sample in the sterile solution is composed of a small number of irregular dimples, and a large number of cracks of approximately 100 μm are observed on the side. However, in the SRB-inoculated solution, the fracture shows the characteristics of quasi-cleavage fracture, and substantial corrosion is observed at the side crack. The EDS result in Figure 8a of 63.09% Al, 2.53% Cl, and 0.10% S, and in Fig. 8b of 42.36% Al, 2.80% Cl, and 1.55% S show that the concentration of S increases significantly in the SRB-inoculated solution, which might be attributed to SRB metabolic activity. For the H20-treated sample, the fracture of the alloy in the sterile solution is mainly observed as dimples, which are a ductile fracture. In the SRB-inoculated solution, the main fracture is composed of the dimple and the tear zone, which is still a ductile fracture, and the side surface shows obvious characteristics of secondary cracking. The tensile fracture of the H10-treated sample in both solutions is dominated by dimples, and only a few secondary microcracks are observed on the side of the sterilized solution. As the ageing rate decreases, the effect of sulfate-reducing bacteria on the tensile properties of heating ageing-treated alloys decreases gradually.

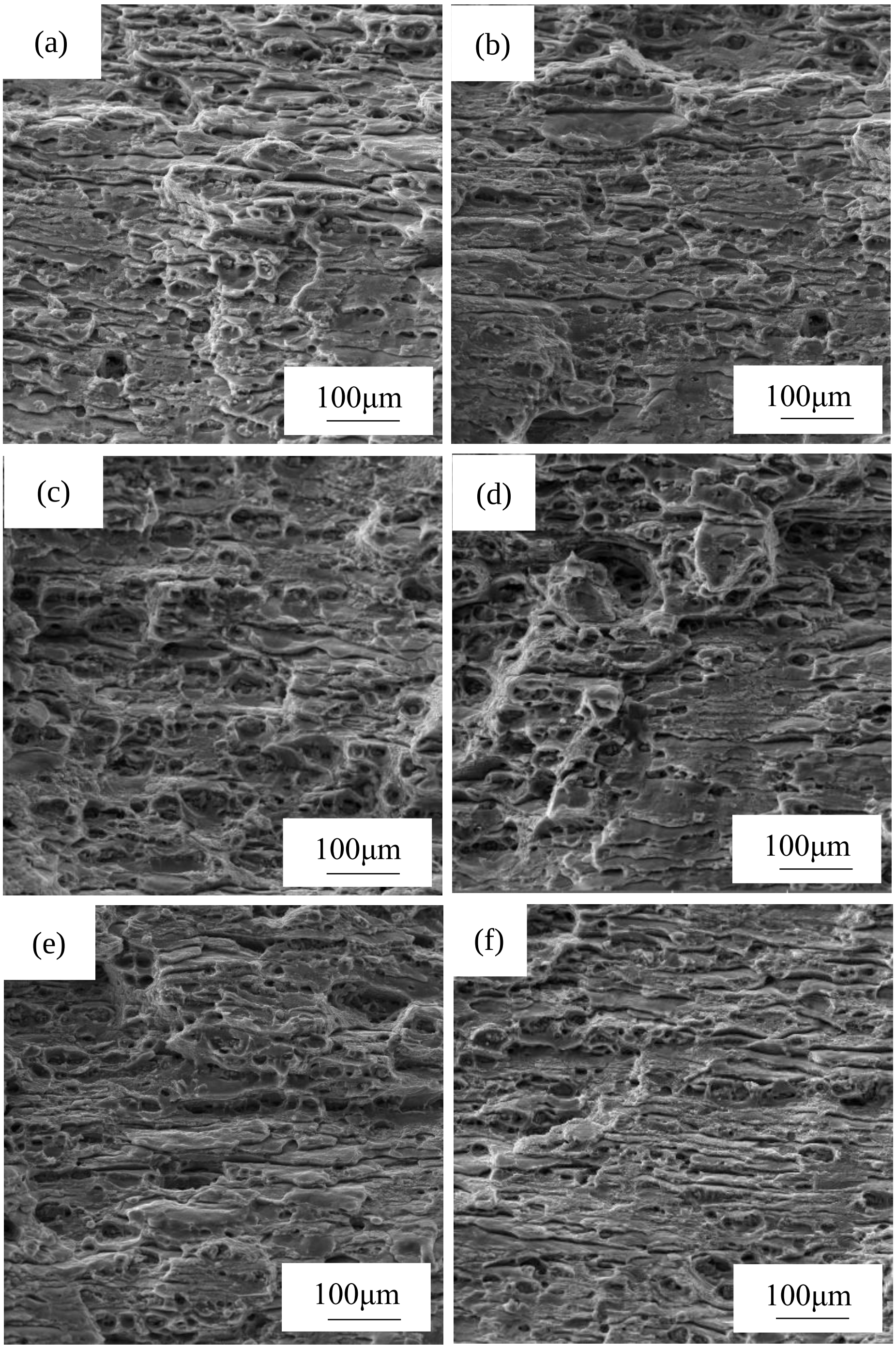

Figure 7. Fracture morphologies of heating aged alloy in solutions: (a) H40 sterile solution, (b) H40 SRB solution, (c) H20 sterile solution, (d) H20 SRB solution, (e) H10 sterile solution, and (f) H10 SRB solution.

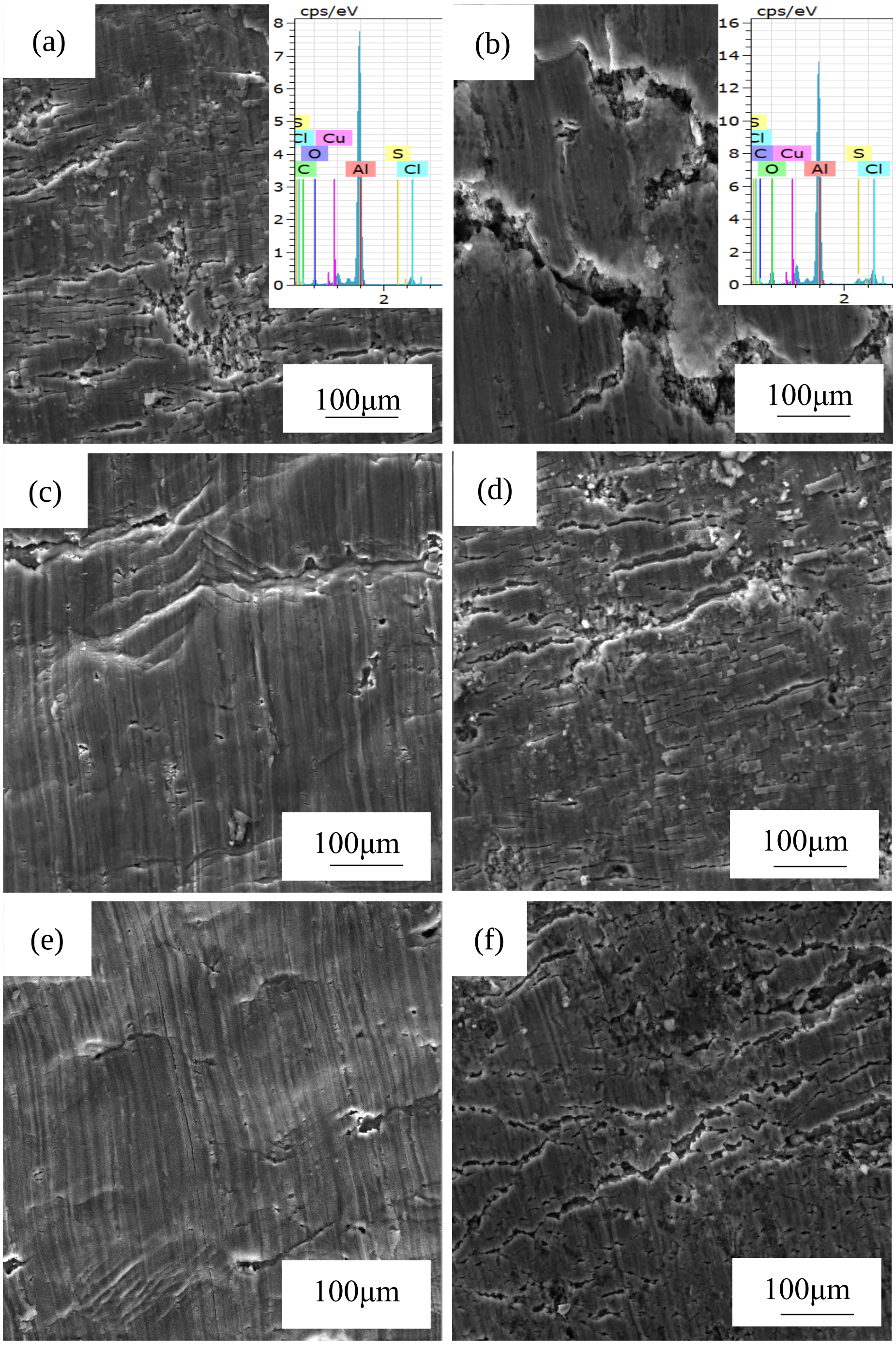

Figure 8. The lateral fracture morphologies and EDS of heating aged alloys in solutions: (a) H40 sterile solution, (b) H40 SRB solution, (c) H20 sterile solution, (d) H20 SRB solution, (e) H10 sterile solution, and (f) H10 SRB solution.

4. DISCUSSION

4.1 SCC sensitivity

The evaluation index I_{scc} includes the expansion area; however, hydrogen produced by the metabolism of SRB in the solution causes abnormal elongation [28]. Thus, the stress corrosion cracking susceptibility is measured by the reduction in area. The I_{scc} is calculated using the following equation [29]:

$$I_{scc} = (1 - \psi_s/\psi_a) \times 100\% \qquad (1)$$

where ψ_s is the reduction in area in corrosion solutions and ψ_a is the reduction in area in air.

As shown in Eq. 1, the closer the value of I_{scc} is to 100, the more susceptible the material is to SCC. The reduction in the area is included in Eq. 1 to obtain the stress corrosion sensitivity of the heating ageing-treated alloy in sterile and SRB-inoculated solutions, as shown in Table 2. In the sterile solution, as the ageing rate decreases, the I_{scc} values of the alloys are 25%, 19.6% and 17.3%, respectively. Compared with the sterile solution, the I_{scc} value of the alloy in SRB-inoculated solution increases by 10%, 5.4% and 4.5%, respectively. The presence of SRB increases the stress corrosion sensitivity of the alloy, and the H10 ageing-treated samples are the least susceptible to SCC among the tested samples.

Table 2. I_{SCC} values of alloys after different aging treatments in sterile and SRB-inoculated solutions.

Process	I_{scc} (Without SRB solution) (%)	I_{scc} (SRB solution) (%)
H40	25±0.6	35±0.5
H20	19.6±0.8	25±0.35
H10	17.3±0.2	21.8±0.25

4.2 Effect of the microstructure on the SCC behaviour

Stress corrosion resistance is one of the main properties of materials and it also difficult to quantify. It is generally believed that SCC resistance increases with the increase of conductivity. The SCC resistance increases with the increase in conductivity. Conductivity is mainly related to a number of factors, such as the vacancy concentration, solute concentration, and the size and volume fraction of the phase [30]. The improvement of conductivity in the ageing process is ascribed to the continuous formation of precipitated phases. During the ageing process, the formation and growth of precipitates will reduce the solute concentration in matrix, therefore, the increase of the conductivity of over ageing alloys is due to the reduction of electron scattering and the number of dissolved atoms caused by the coarsening of precipitations [31]. In Fig. 3b, the conductivity increases with the decrease in the ageing rate.

the formation and growth of precipitates will the solute concentration in the matrix.,

is attributed to the continuous formation of precipitated phase.During the aging process, the formation and growth of the precipitate will decrease the solute concentration in the matrix.Therefore, the increase in conductivity in overaged alloys is due to the reduction in electron scattering and the coarsening of precipitation resulting in a decrease in the number of dissolved atoms

After the ageing treatment, the microstructural characteristics of the Al-Zn-Mg-Cu alloy, such as the type, size and distribution of matrix and grain boundary precipitates and the width of PFZ, have changed, which exert important effects on its mechanical properties and stress corrosion [32]. According to a previous report, SCC occurs in an ordinary Al alloy system via an anodic dissolution model rather than mechanical fracture model [33]. The stress corrosion cracking of an aluminium alloy with high strength generally expands along the grain boundary, and thus the chemical properties of grain boundary play an important role in stress corrosion. Microstructures of alloys were further investigated with TEM to elucidate the SCC mechanism.

In the under-aged alloy (e.g., H40 treatment), the number of intracrystalline precipitates is small and fine, and the grain boundaries are filled with equilibrium phase forming continuous GBPs, as shown in Fig. 9a. At this time point, the effect of precipitation strengthening is weak, and dislocation clogging easily occurs at the continuous grain boundaries; thus, the strength and elongation of the alloy are reduced. GBPs generally serve as anodes and dissolve during galvanic interactions because of the difference in potential between the aluminium matrix and GBPs. Therefore, corrosion occurs preferentially at the grain boundary and eventually forms a corrosion channel along the continuous GBPs, the occurrence of SCC is reasonable. In Fig. 8b, a large number of corrosion cracks on the side of the fracture, inducing stress corrosion cracking. Based on this analysis, the SCC fracture behaviour of the H40-treated alloy in characteristic region is explained by the anodic dissolution theory at the grain boundary.

As the ageing rate decreases, the coarse and wide η phase distributed discontinuously along the grain boundary would not become a network of corrosion channels, which reduces the susceptibility to intergranular corrosion with an associated resistance to stress corrosion cracking. Moreover, the equilibrium phase causes the alloying elements to use up at the grain boundary, and the loss of solute atoms is not supplemented, resulting in the formation of PFZ along the grain boundary. When a slip zone crosses on grain boundaries during plastic deformation, the accumulation of dislocation in the slip zone produces local stress concentration. The PFZ results in an increase in ductility, since the PFZ relaxes the stress concentrated at the end of the slip band [34]. According to this argument, it is possible to improve ductility because most of the local stress concentration is relaxed at PFZs as they become wider after an over-aging treatment. However, the presence of a large phase in the matrix promotes the nucleation of a crack during the plastic deformation process.

The stress reaches a critical value between the large precipitation and matrix where causes the formation of interfacial cracks, the σ for precipitate cracking is calculated using the following equation [35]:

$$\sigma = (6E\gamma/q^2r)^{1/2} \qquad (2)$$

where E is Young's modulus of the precipitate, γ is the surface energy of the precipitate, q is the stress concentration factor at the precipitate, and r is the precipitate radius. The larger size of the precipitate phase might lead to a greater stress concentration. Based on Eq. (2), larger precipitates are associated with a lower critical stress. Therefore, the main stress corrosion mechanism of the alloy is anodic dissolution near the thick phase when the ageing rate is low.

4.3 Effect of SRB on the SCC behaviour

In the sterile medium, the film of corrosion product absorbs the compounds in the solution function as a barrier that prevents the permeation of corrosive ions. The EIS results of the fracture process show that the presence of SRB decrease the resistance and increase the corrosion rate of the alloy compared with the sterile solution.

In the SRB-inoculated medium, SRB attached to the Al alloy electrode surface exhibit normal metabolism to produce extracellular polymeric substances (EPS), which consist of proteins, carbohydrates, organic acids, and other substances. SRB potentially participate in the electron transfer process that typically uses SO_4^{2-} as an electron acceptor, which is shown in Fig. 9. SRB use enzymes to reduce SO_4^{2-} to H_2S, HS^- and S^{2-} [36,37]. Consequently, the bacteria prevent the hydrogen atoms from forming hydrogen molecules, thus promoting their diffusion into the interior of the material. According to the SSRT results, compared with the sterile solution, the presence of SRB reduces the yield strength and elongation of the tested alloys; meanwhile, cracks are generated on the side of the fracture, and increase the susceptibility to SCC. H_2S is a catalyst for hydrogen penetration that effectively accelerates the hydrogen permeation into the interior of the alloy; however, the hydrogen permeation of metal materials reduces the cohesive energy and toughness of the material, and an alloy is considerably more susceptible to SCC behaviour [38]. In fact, studies by Javaherdashti [39] have shown that sulfide plays a toxic role in the bonding process of hydrogen atoms, thus promoting their diffusion into the metal and causing embrittlement. Hydrolyzed by the metabolites, hydrogen diffused into the metal, and with the action of stress, hydrogen atoms continued to accumulate in the high-stress area at the crack tip. The hydrogen concentration, hydrogen pressure and stress intensity factor in the crack tip area increased exponentially over time, increasing the hydrogen embrittlement sensitivity in the metal [40]. Therefore, the main SCC mechanism of the alloy in SRB inoculation solution is hydrogen-induced cracking (HIC).

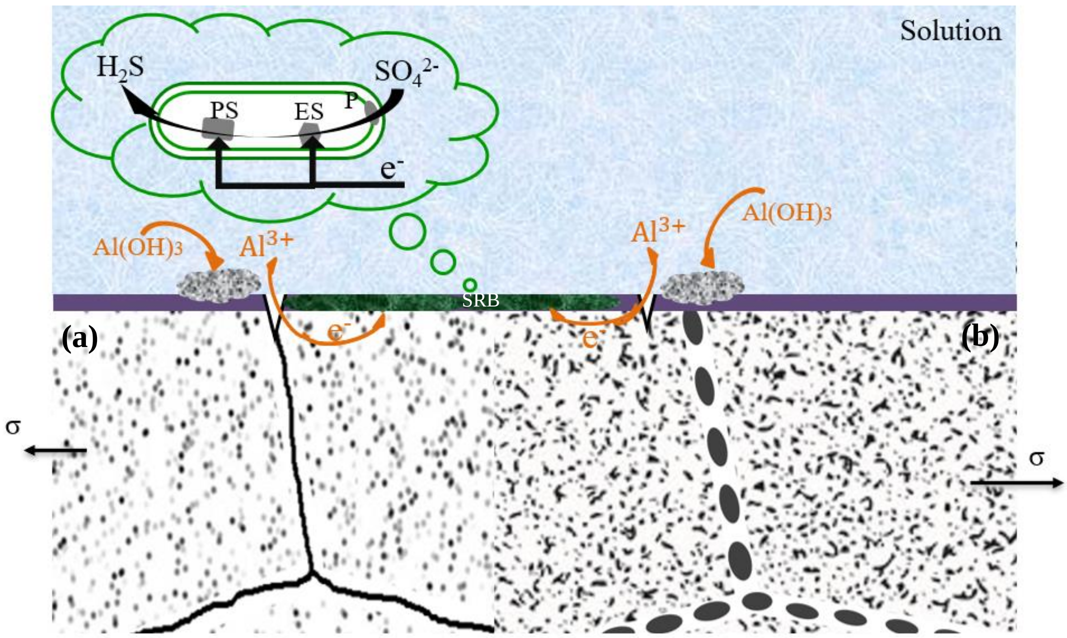

Figure 9. Schematic of the SCC mechanism for the Al alloy in SRB-inoculated solution: (a) GBPs continuous, and (b) GBPs grow up and intermittent. The scheme indicates specific proteins (P) in the outer membrane allow electron transport to the enzymes for sulfate reduction, enzyme for sulfate activation (ES), and protein for sulfate uptake (PS).

5. CONCLUSIONS

Heating ageing-treated Al-4.47Zn-2.13Mg-1.20Cu alloy samples were exposed to a corrosion solution under the effect of an applied stress to investigate the role of SRB in the SCC process. Through electrochemical experiments and microscopy techniques, the conclusions listed below were drawn.

(1) The SCC resistance of the Al-Zn-Mg-Cu alloy is obviously improved by decreasing the heating ageing rate. When the ageing rate is 10°C/h, the sample exhibits the highest charge transfer resistance and the least stress corrosion cracking sensitivity (I_{scc}).

(2) When the heating rate is fast, the precipitated in matrix is fine and continuous at the grain boundary; as well as lower heating rate, the radius of precipitation increases rapidly and GBPs are intermittent distribution with a PFZ that effectively prevent from undergoing anodic dissolution.

(3) The corrosion rate of the aluminium alloy is accelerated substantially by SRB, and the main stress corrosion mechanism of the alloy shifted from anode dissolution to hydrogen-induced cracking.

ACKNOWLEDGEMENTS
The authors gratefully acknowledged the sponsorship from the National Natural Science Foundation of China (NO. 51574147 and NO. 51790481) and the Liaoning Provincial Natural Science Foundation of China (NO. 201602474).

References

1. T.Q. Wu, M.C. Yan, D.C. Zeng, J. Xu, C.K. Yu, C. Sun, and W. Ke, *Acta Metall. Sin.*, 28 (2015) 93.
2. M.A. Javed, P.R. Stoddart, E.A. Palombo, S.L. Mcarthur, and S.A. Wade, *Corros. Sci.*, 86 (2014) 149.
3. C. Xu, Y. Zhang, G. Cheng, and W. Zhu, *Mater. Charact*., 59 (2008) 245.
4. D.X. Sun, M. Wu, and F. Xie, *Mater. Sci. Eng. A*, 721(2018) 135.
5. S. Chen, P. Wang, and D. Zhang, *Corros. Sci.*, 87 (2014) 407.
6. M.A. Krishnan, and V.S. Raja, *Corros. Sci.*, 109 (2016) 94.
7. K. Ma, T. Hu, and H. Yang, *Acta Mater.*, 103 (2016) 15.
8. M. Wu, Z.H. Zhao, X. Wang, J.C. Huang, and X.Y. Liu, *Int. J. Electrochem. Sci.*, 15 (2020) 208.
9. Y.R. Liu, Z.Z. Dong, L.M. Yu, Y.C. Liu, and H.J. Li, *J. Mater. Res.*, 30 (2015) 179.
10. F. Guan, X.F. Zhai, J.Z. Duan, J. Zhang, K. Li, and B. Hou, *Surf. Coat. Technol.*, 316 (2017) 171.
11. Q.L. Zhang, Z.Q. Hu, W.W. Su, H.L. Zhou, C.X. Liu, Y.L. Yang, and X.W. Qi, *Surf. Coat. Technol.*, 321 (2017) 64.
12. Z.Y. Cui, Z.Y. Liu, and L.W. Wang, *Mater. Sci. Eng. A*, 677 (2016) 259.
13. X. Xin, X.M. Zhang, S.D. Liu, F.X. Song, and B. Chen, *J. Mater. Eng.*, 63 (2014) 29.
14. X.Y. Liu, M.J. Li, F. Gao, S.X. Liang, X.L. Zhang, and H.X. Cui, *J. Alloys Compd.*, 639 (2015) 263.
15. Y.P. Xiao, Q.L. Pan, W.B. Li, X.Y. Liu, and Y.B. He, *Mater. Corros*., 63 (2012) 421.
16. K.R. Prasanta, M.M. Ghosh, and K.S. Ghosh, *J. Mater. Eng. Perform*, 24 (2015) 2792.
17. S.H. Wang, X.G. Zhang, and S.J. Yang, *Rare Met.*, 29 (2010) 433.
18. D.K. Xu, N. Birbilis, and P.A. Rometsch, *Corros. Sci.*, 54 (2012) 17.
19. M. Baydogan, H. Cimenoglu, E.S. Kayali, and J. Rasty, *Metall. Mater. Trans. A*, 39 (2008) 2470.
20. A.F. Oliveira, M.C.D. Barros, K.R. Cardoso, and D.N. Travessa, *Mater. Sci. Eng. A*, 379 (2014) 321.
21. X. Peng, Y. Li, X. Liang, Q. Guo, G.F. Xu, and X.Y. Peng, *J. Alloys Compd.*, 735 (2018) 964.

22. X.Y. Peng, Q. Guo, X.P. Liang, Y. Deng, Y. Gu, and G. Xu, *Mater. Sci. Eng. A*, 688 (2017) 146.
23. D.M. Jiang, Y. Liu, S. Liang, and W.L. Xie, *J. Alloys Compd.*, 681 (2016) 57.
24. D. Wang, F. Xie, M. Wu, D.X. Sun, Q.H. Zhao, and L.S. Cheng, *Mater. Mech. Eng.*, 40 (2016) 57.
25. J. Chen, J. Wu, P. Wang, D. Zhang, S.Q. Chen, and F.Q.Tai, *J. Mater. Eng. Perform.*, 28 (2019) 1469.
26. A.L. Ning, Z.Y. Liu, C. Feng, and S.M. Zeng, *Trans. Mater. Heat Treatment*, 29 (2008) 108.
27. Y.A.N. Maocheng, X.U. Jin, and Y.U. Libao, *Corros. Sci*., 110 (2016) 23.
28. H.C. Ma, Z.Y. Liu, C.W. Du, H.R. Wang, C.Y. Li, X.G. Li, *Mater. Sci. Eng. A*, 642 (2015) 22.
29. A. Torres-Islas, and J.G. González-Rodríguez, *Int. J. Electrochem. Sci.*, 4 (2009) 640.
30. I.B. Kim, K.N. Kim, K.H. Kim, and I.G. Kim, *Mater. Sci. Forum*, 449-452 (2014) 585.
31. X. Chen, S. Zhai, D. Gao, Y. Liu, J. Xu, and Y. Liu, *Mater. Res. Express*, (2018) 1.
32. G.S. Peng, K.H. Chen, S.Y. Chen, and H.C. Fang, *Mater. Corros*., 63 (2012) 254.
33. D. Najjar, T. Magnin, and T.J. Warner, *Mater. Sci. Eng. A*, 238 (1997) 293.
34. Park D S, and Nam S W. *Mater. Sci. Technol.*, 11 (1995) 921.
35. T.S. Srivatsan. *J. Mater. Sci.*, 27 (1992) 4772.
36. H.C. Ma, Z.Y. Liu, C.W. Du, H.R. Wang, X.G. Li, D.W. Zhang, and Z.Y. Cui, *Corros. Sci.*, 100 (2015) 627.
37. T.Q. Wu, J. Xu, C. Sun, M.C. Yan, C.K. Yu, and K. Wei, *Corros. Sci.*, 88 (2014) 291.
38. S. Chen, P. Wang, and D. Zhang, *Corros. Sci.*, 87 (2014) 407.
39. R. Javaherdashtia, R.K.S. Ramanb, and C. *Panterc, Int. Biodeter. Biodegr.*, 58 (2006) 27.
40. J. Song, and W.A. Curtin, *Acta Mater.*, 59 (2011) 1557.